Journal of Manufacturing Processes 156 (2025) 13–28

Contents lists available at ScienceDirect

Journal of Manufacturing Processes

journal homepage: www.elsevier.com/locate/manpro

Reducing energy consumption of pulsed-gas metal arc additive manufacturing through machine learning algorithms

Giulio Mattera [a,*], Zengxi Pan [b], Luigi Nele [a], Vittoria Laghi [c]

[a] Department of Chemical, Materials and Industrial Production Engineering - University of Naples Federico II, Italy
[b] School of Mechanical, Materials, Mechatronic and Biomedical Engineering - University of Wollongong, NSW, Australia
[c] Department of Civil, Chemical, Environmental and Materials Engineering – University of Bologna, Italy

ARTICLE INFO

Keywords:
Additive manufacturing
Genetic algorithm
Sustainability
Energy consumption
Optimisation

ABSTRACT

Gas Metal Arc Additive Manufacturing (GMA-AM), also known as Wire Arc Additive Manufacturing (WAAM), has gained significant attention from both industry and academia due to its cost-effectiveness and capability to produce medium- to large-scale metal components. While previous research has mainly focused on the effect of process parameters on the final part properties, this study explores how Artificial Intelligence (AI) can support parameter selection to improve part quality and energy efficiency. An AI-based optimisation framework integrating regression and classification models is proposed to predict and optimise layer geometry, power consumption, and deposition quality. Experimental data from 72 layers of 316 stainless steel deposited via a pulsed GMAW process are used to train a Gaussian Process Regression (GPR) model that estimates electrical power and layer geometry from process parameters. A Random Forest Classifier (RFC) identifies parameter combinations leading to non-compliant layers, while a sustainability-oriented fitness function is optimised using a Genetic Algorithm (GA). The proposed framework achieves a 14.4 % reduction in input energy without compromising layer quality and demonstrates a 15 % energy saving in the fabrication of a test component.

1. Introduction

Additive Manufacturing (AM) has emerged as a disruptive set of technologies with the potential to transform manufacturing processes by offering flexibility and high customisation in production with minimal human intervention [1]. Among mid- to large-scale metal AM, interest is growing around Gas Metal Arc Additive Manufacturing (GMA-AM), also known as Wire Arc Additive Manufacturing (WAAM). Thanks to its reduced costs and production time with respect to other metal AM processes (such as Powder Bed Fusion, PBF), WAAM is largely employed in aerospace, maritime, and oil & gas industries [2,3]. This process uses Gas Metal Arc Welding (GMAW) processes [4] to additively manufacture metal components in a layer-by-layer fashion. In particular, a robotic arm is equipped with a welding machine, while a slicer software generates the robotic code for the motion and the program to set the process parameters on the welding machine. Moreover, aiming to meet Industry 4.0 requirements in terms of intelligent applications such as feedback control [5–8] and process monitoring [9–11], several sensors are integrated, adding an additional element called Welding Monitoring System (WMS). The process and the equipment are shown in Fig. 1.

Despite the growing interest in this technology, as-built components are still affected by several issues, such as dimensional accuracy, surface quality, and internal defects, which significantly hinder its widespread adoption [12,13]. To address these challenges, process monitoring [14–18] and control [19–21] represent mandatory steps, and numerous applications have been developed in this regard. However, process optimisation (optimal path and parameters generation step in Fig. 1) also plays a crucial role, as it allows the identification of optimal parameters before implementing real-time monitoring and control strategies. Although monitoring and control are essential for certifiable GMA-AM processes, starting from an optimised baseline remains fundamental to further improving the final part quality.

1.1. Sustainability through energy efficiency: a growing topic in AM

The research trend in the field of WAAM can be divided into three different stages following the study of He et al. [22]. From 2010 to 2013, the research focused on the material properties, while from 2014 to

* Corresponding author.
E-mail address: giulio.mattera@unina.it (G. Mattera).

https://doi.org/10.1016/j.jmapro.2025.11.034
Received 16 October 2025; Received in revised form 11 November 2025; Accepted 12 November 2025
1526-6125/© 2025 The Authors. Published by Elsevier Ltd on behalf of The Society of Manufacturing Engineers. This is an open access article under the CC BY license (http://creativecommons.org/licenses/by/4.0/).

2017 most of the literature focused on the process control and parameter optimisation for quality parts fabrication. Nowadays, the trends rely on the application of Artificial Intelligence (AI), aiming to develop intelligent production systems, according to Industry 4.0 requirements [23]. As outlined in the United Nations Sustainable Development Goals Report 2023, "Goal 12 Responsible Consumption and Production" aims to ensure sustainable consumption and production patterns. In the context of WAAM, the environmental impact is largely influenced by fume emissions, shielding gas consumption, and energy use [24]. For this reason, over the last year, a new research path on sustainable and energy-efficient production in AM has interested the research community [25]. Previous studies demonstrated that GMA-AM (or WAAM) is characterised by high energy efficiency [26–29], resulting in lower carbon emissions when compared to low-efficiency AM technologies based on laser or plasma [30]. Additionally, recent work compared the cost associated with GMA-AM to traditional manufacturing [29,31], revealing potential also for cost savings when adopted to realise complex-shaped geometries. Similar research has also been conducted comparing GMA-AM with LPBF technology [32] and CNC milling [33]. Although it has been demonstrated that GMA-AM technology is inherently a sustainable process compared to other AM technologies for metal parts, the present work proposes an optimisation process consisting of depositing different layers with different parameters and selecting the one that minimises power consumption and surface roughness, which inherently depends on the layer geometry [34].

1.2. Process optimisation methods for additive manufacturing

Optimisation procedures play a pivotal role in numerous scientific and engineering domains, guiding the design and refinement of systems to achieve the desired objectives. Traditionally, process engineers rely on extensive experimental campaigns to identify optimal parameter combinations. However, this approach is inherently limited, as it is not feasible to experimentally explore all possible process conditions. Nevertheless, in the AM literature, [34,35], and particularly for GMA-AM [36–41], the optimisation procedure still largely depends on empirical evidence, where parameters are iteratively tuned through experiments. While effective to some extent, such methods demand substantial time and resources and struggle to identify non-intuitive or high-dimensional solutions, especially in complex multi-input/multi-output processes. These limitations highlight the need for data-driven approaches that can complement and enhance traditional optimisation practices.

In this regard, the integration of AI into optimisation procedures can offer various advantages. Firstly, AI can expedite the optimisation process by rapidly evaluating numerous configurations and identifying promising candidates for further exploration. Additionally, AI can discover non-intuitive solutions that may not be apparent through traditional experimental methods, leading to breakthroughs and advancements in various fields. Several examples in GMA-AM of ML-based optimisation can be found. For example, Gihar et al. [42] proposed a neural network model for estimating the bead width and shape, which was then used to optimise the path-planning parameters for corner structures. The potential offered by Machine Learning (ML) models has generally been exploited for simulation-based optimisation [43]. However, rather than randomly exploring the parameter space, bio-inspired algorithms can be employed to efficiently and systematically search the process space, with the aim of optimising a given cost or fitness function. In this context, AI tools such as Reinforcement Learning (RL) [44] or metaheuristic methods such as Genetic Algorithm (GA) [45] and Particle Swarm Optimisation (PSO) [46] supported by regression models such as Neural Networks and Support Vector Machine [47,48] can be used. A relevant example developed for GMA-AM technology is the work of Kumar et al., in which the authors adopted a discrete GA addressing a 3-level with 4 parameters optimisation problem [49]. The objective was to maximise material yield and minimise the occurrence of voids in the printed component. Despite this effort, the existing literature lacks applications of optimisation methods specifically tailored for the GMA-AM process from a cost-saving and energy-efficient perspective. A comparison between the standard optimisation procedure and AI-enabled model-based optimisation procedure is shown in Fig. 2.

Moreover, in AM—and especially in GMA-AM—not all parameter combinations are physically valid, as many lead to instabilities or defect formation. Previous studies, such as the work of Le et al., have addressed this issue by manually constraining the process parameter space around known "safe" regions [50]. While this reduces the risk of defects, such manual constraints often lead to suboptimal optimisation, as they restrict the search space and prevent the discovery of potentially superior solutions, highlighting the need for new methodological solutions capable of addressing these challenges within GMA-AM optimisation.

1.3. Research gap and work proposal

A common limitation of these studies is their exclusive reliance on regression models combined with GA for optimisation. This approach typically does not incorporate classifiers capable of evaluating whether a given combination of parameters has previously resulted in defects or instability. As a result, such potentially problematic combinations are

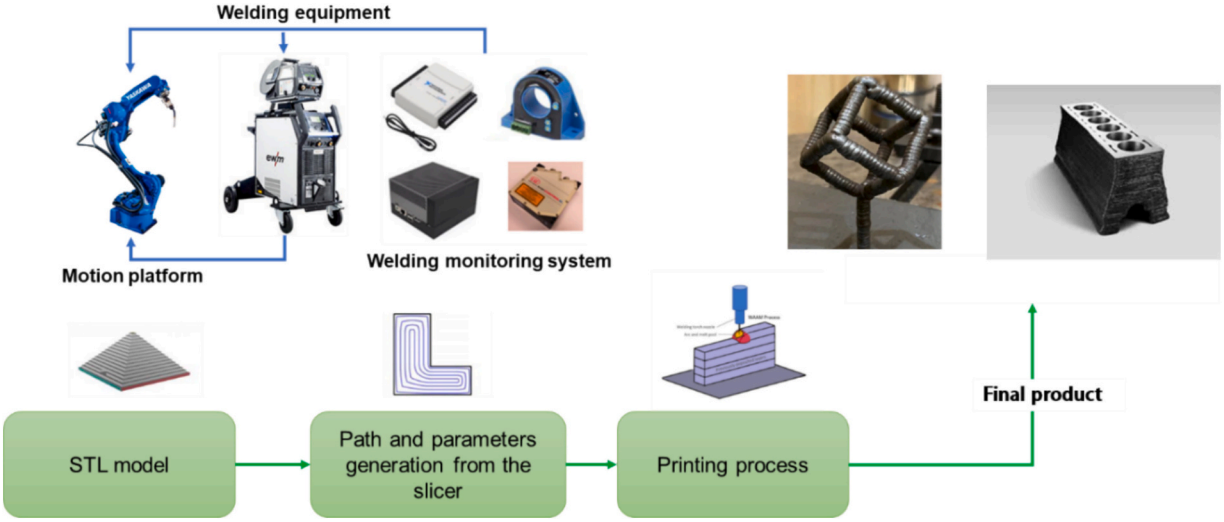

Fig. 1. GMA-AM process workflow: from the STL model to the final product.

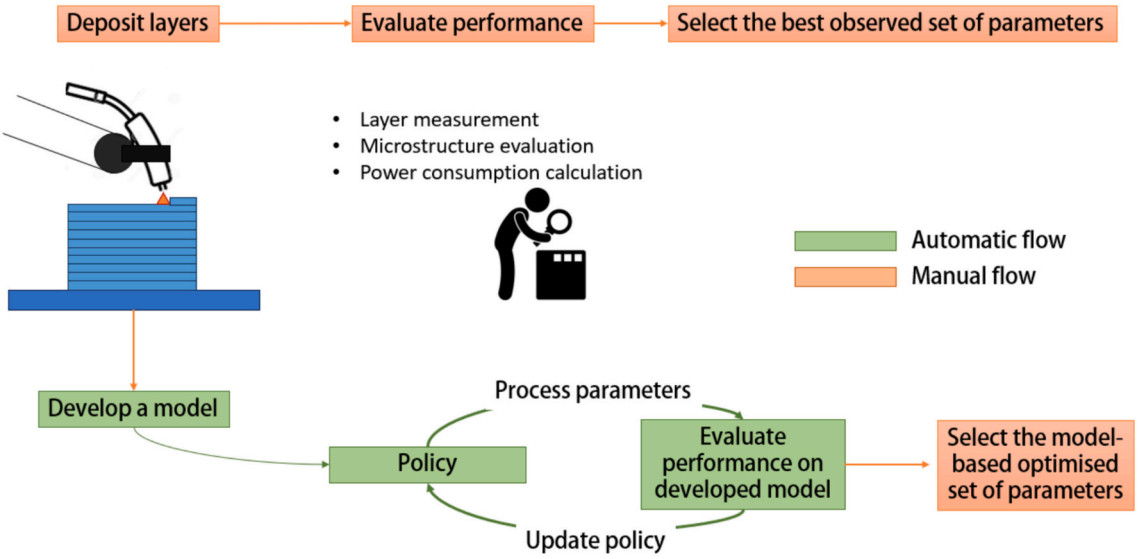

Fig. 2. Comparison between experiment-based optimisation and AI-enabled model-based optimisation procedures.

excluded from the search, thereby restricting the parameter space to configurations already known to produce high-quality outcomes [51]. While this increases the complexity of the optimisation procedure, it may enable the identification of suitable process parameters outside the initially constrained space.

Moreover, regarding the design of the fitness function, the objectives proposed in the literature typically focused on optimising either the mechanical properties of the printed parts or their printing rates. However, only few studies considered sustainability factors into account, such as energy consumption [51]. Given this research gap, this research work proposes three principal novelties in GMA-AM data-driven optimisation:

- A new AI-based optimisation framework that incorporates information on power consumption and deposition quality into the optimisation loop through the mutual utilisation of regression and classification models;
- This approach enables the automatic constraint of process parameter combinations that lead to unstable or low-quality depositions, reducing the need for manual exclusion of unfeasible operating conditions, typical of state-of-the-art methods.
- A novel sustainability-oriented fitness function for GMA-AM is proposed, which links power consumption to the indirect optimisation of surface quality, material efficiency and specific energy consumption, through process-dependent parameters such as wire feed speed.

Altogether, the integration of the proposed sustainability-oriented fitness function with the ensemble data-driven procedure enables the automatic generation of process parameter sets that produce stable and defect-free depositions, thereby ensuring high-quality outcomes and extending the optimisation beyond conventional performance-driven formulations and assure energy savings. In this work, the experimental setup, data collection procedure, and proposed methodology are described in Section 2. The results of applying the proposed methodology for process parameter optimisation are presented in Section 3, where different techniques are compared. Section 4 discusses the validation of the results on multi-bead, multi-layer components, highlighting the achieved energy savings and quality improvements obtained through the proposed approach, along with a discussion of potential future developments of this research.

2. Materials and methods

Following the procedure outlined in Fig. 2, a set of experimental tests was conducted to collect data to develop a ML model. This model is designed to estimate layer geometry (including layer width and height), layer quality and power consumption based on process parameters. A GA is subsequently employed to automatically search for optimal process parameters, with the objective of maximising a defined fitness function.

2.1. Experimental setup

The configuration of the experimental system comprises a Yaskawa AM2010 robotic station integrated with a Lincoln PowerWave 500 welding equipment. The WMS comprises a Micro-Epsilon 2500 laser profilometer, used to measure the bead geometry after deposition and current and voltage sensors connected to a National Instruments 6003 device, used to compute the average power consumed during each deposition. To ensure consistency in the evaluation, 72 layers of stainless steel 316 L were deposited using a 1.2 mm wire over 70 mm paths on a stainless-steel substrate through a synergic Pulsed Gas Metal Arc Welding (P-GMAW) process. The experimental conditions, summarised in appendix in Table A.1, involved varying the wire feed speed, welding speed, arc voltage, and the UltimArc parameter controlling the pulse frequency of the Lincoln system. The shielding gas was a mixture of 80 % Argon and 20 % Carbon Dioxide at a constant flow rate of 22 L/min, while the Contact Tip to Workpiece Distance (CTWD) was fixed at 15 mm. Once all the single layers were deposited, the collected data were processed as detailed in the following sections. An ensemble of ML models was then developed using the previously acquired information on power consumption and layer quality. These models were integrated within a GA-based optimisation framework, enabling the automatic optimisation of process parameters. The optimised parameters were subsequently validated through the deposition of a test component to assess model reliability and process repeatability. The overall workflow of the study is summarised in Fig. 3 and described in detail in the subsequent sections.

The final deposited layer quality was classified by an expert welder based on the layer appearance, the amount of spatter, and the sound generated during deposition. More specifically, layers exhibiting surface defects such as humping or porosity have been classified as anomalous (see Fig. 4). Humping [52] can introduce changes into CTWD which can generate instability and out-of-specification welds, while porosity could

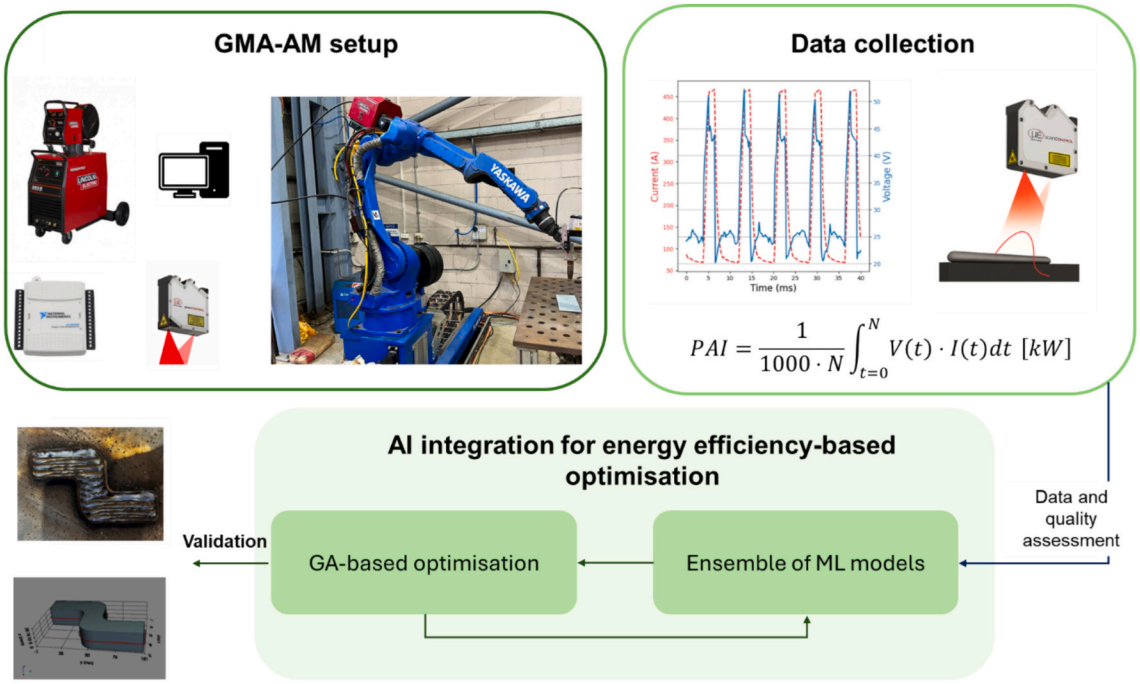

Fig. 3. Experimental setup and AI-driven optimisation framework integrating data acquisition, ML-based process modelling, and GA optimisation for automatic parameter tuning considering energy efficiency and deposition quality.

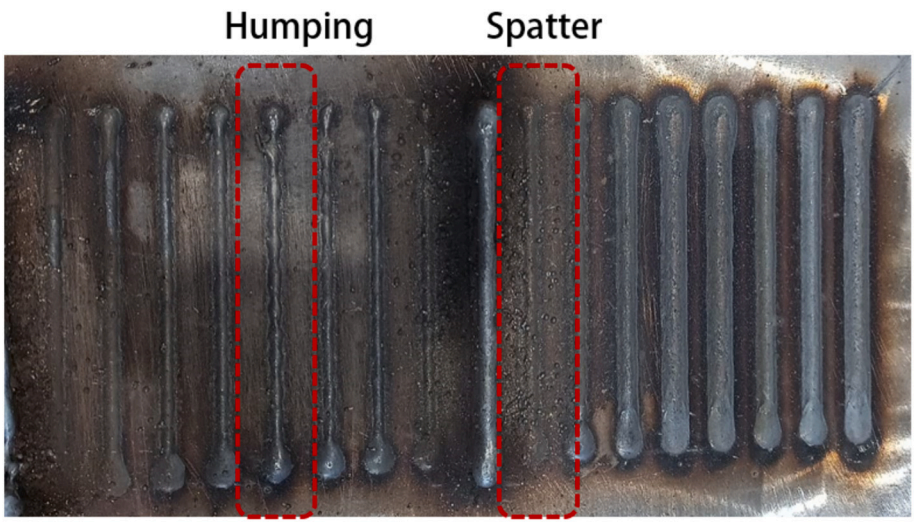

Fig. 4. Examples of excessive spatter and humping defects observed during layer deposition.

significantly reduce the mechanical properties. Additionally, since welding sound is closely associated with arc stability and spatter [53], layers displaying excessive instability or spatter, such as explosive behaviour or the presence of spatter on the surface, were also classified as anomalous, due to inconsistency of heat input [54]. Moreover, excessive spatter during welding can reduce the lifespan of the nozzle and lead to poor shielding gas coverage, ultimately resulting in porosity. Similarly, an explosive arc indicates an unstable and poorly controlled process, which can also lead to defects such as porosity.

2.2. Data collection

The recorded values of welding current and voltage allowed for the evaluation of the average power consumption during the deposition process. In waveform-controlled welding, particularly in the production of parts through the GMA-AM process, obtaining an accurate measure of power and energy requires instantaneously measuring the electrical parameters. As proposed by Joseph et al. [55], the average instantaneous power (*PAI*) is expressed by Eq. 1, where V is the instantaneous welding voltage, I is the instantaneous welding current, and N is the number of time intervals considered for the evaluation of *PAI*.

$$PAI = \frac{1}{1000 \cdot N} \int_{t=0}^{N} V(t) \cdot I(t) dt \ [kW] \quad (1)$$

ISO/TR 18491 advises a sampling rate of at least 10 times the waveform frequency, requiring the use of acquisition systems capable of providing sample rates of at least 5 kHz, as employed in the data collection procedure [56]. The instantaneous power, computed as the product of the welding current and voltage signals representing the arc energy, was adopted as the primary metric for process power

consumption. The contribution of the robotic manipulator to the overall energy demand was neglected, given that it operated at only 5–10 % of its nominal speed, corresponding to less than 5 % of the total process power. Notably, the robot's maximum power consumption at full operational speed is approximately an order of magnitude lower than the welding power. This assumption is technically sound and consistent with common practice in life cycle assessment studies of arc-based additive manufacturing systems [57,58]. The hardware employed in this study consists of a NI-6009USB acquisition board, connected via serial communication to a workstation. Using the NI-DAQmx Python library, it was possible to collect data online during the deposition process, from which the *PAI* associated with the deposition was evaluated. The final bead geometry of all 72 deposited layers was measured post-deposition using a Micro-Epsilon 2500 laser scanner. This sensor provides a measurement accuracy of ±3 μm. For each layer, the bead geometry was evaluated from the measured surface profile data at five distinct cross-sections, and the average values were used in the analysis for both bead width and height.

2.3. Proposed methodology and framework for optimisation

This study proposes an innovative framework for optimising GMA-AM process parameters. As shown in Fig. 5, it combines regression and classification ML models to estimate the deposition outcomes from layer geometry, power consumption, and quality perspectives. A continuous GA agent efficiently explores the parameter space, guided by a fitness function that solves a multi-objective constrained optimisation problem. The aim is to minimise power consumption without compromising the printed part's layer quality.

The proposed framework integrates both regression and classification models, enabling the optimisation algorithm to identify process parameters that are not only energy-efficient but also defect-free. The regression model (Gaussian Process Regression, GPR) predicts the quantitative process outcomes, such as power consumption and geometric features, while the classification model (Random Forest Classifier, RFC) automatically detects and excludes parameter combinations likely to produce defects. This creates a data-driven constraint mechanism that replaces traditional manual or empirical restrictions with an adaptive, model-based approach. The models' hyperparameters were manually tuned to ensure reliable predictions; however, the framework itself is model-agnostic and can accommodate alternative regression or classification algorithms depending on the specific application or dataset. The selection of GPR and RFC models were deliberately selected for their interpretability, robustness with limited datasets, and low computational cost—key advantages in industrial AM applications where data acquisition is often expensive and time-intensive—whereas deep learning architectures, such as feedforward neural networks, were deemed less suitable given the dataset size nature of the input data.

2.4. Machine learning models employed

2.4.1. Gaussian process regression

Stochastic processes are mathematical models that characterise systems undergoing random changes over time, introducing inherent uncertainty and resulting in multiple potential paths of evolution, even when the initial state is known. In the context of AM processes, such as GMA-AM, uncertainties arise due to complex thermal phenomena during the deposition process, making it suitable for treatment as a stochastic process. Among various stochastic models, Gaussian processes are more commonly utilised [59,60]. These processes are defined by a mean function and a positive-definite covariance function, representing the expected values of the process and the relationships between different points in the input domain, respectively. The Gaussian Process Regression (GPR) method is a nonparametric supervised learning method which considers output values as samples from a multivariate Gaussian distribution, as reported in Eq. 2.

$$f(x) \sim GP(\mu, \Sigma) \tag{2}$$

The prior distribution is established by defining a mean value μ which can be constant and either equal to zero or to the mean of the training data. The prior covariance Σ is shaped by passing a kernel object, and its hyperparameters are optimised through methods like L-BFGS-B [61], maximising the log-marginal-likelihood (LML). The GPR learning process includes the computation of the posterior distribution and the predictions for new data points. The choice of the covariance function, also known as the kernel function, is crucial for incorporating prior information into the model. The kernel function must be positive-definite to serve as a valid covariance function, and it defines the similarity between data points. In this work, to capture white noise in the data, a white noise kernel is employed, reported in Eq. 3, where σ is a scaling factor, representing the variance of the white noise and $x_i, x_j$are the data points being compared in the kernel function. In this work, σ is set equal to 1.

$$k_1(x_i, x_j) = \begin{cases} \sigma & if\ x_i == x_j \\ 0 & if\ x_i \neq x_j \end{cases} \tag{3}$$

Additionally, the Radial Basis Function (RBF) kernel function (Eq. 4) is used to constrain the model extrapolations within a distance from the training data equal to L. In this work, L is set equal to 1.

The linear kernel (Eq. 5) is then adopted to address the linear dependencies between variables. This latter aspect has been also previously evidenced in literature in terms of correlations between layer width, layer height, wire feed speed and welding speed [62].

$$k_2(x_i, x_j) = e^{-\frac{1}{2L^2}||X_i - X_j||^2} \tag{4}$$

$$k_3(x_i, x_j) = x_i \cdot x_j + \sigma^2 \tag{5}$$

Data normalisation precedes the training phase, ensuring a consistent and effective modelling approach. A weighted approach is adopted,

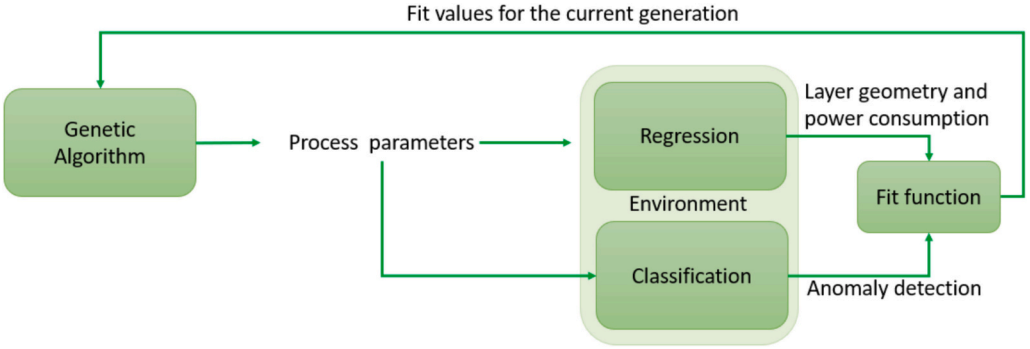

Fig. 5. The proposed optimisation framework.

assigning more importance (weight $w = 0.5$) to the RBF kernel and less importance (weight $w = 0.25$) to the linear relationship and noise model. The final kernel used in this study is reported in Eq. 6.

$$k(x_i, x_j) = 0.25 \cdot k_1(x_i, x_j) + 0.25 \cdot k_2(x_i, x_j) + 0.5 \cdot k_3(x_i, x_j) \quad (6)$$

2.4.2. Random Forest Classifier

As discussed, during the conducted experimental investigations, certain parameter combinations resulted in excessive spatter or defects during the deposition process, as shown in Fig. 6. Identifying and avoiding these sets of parameters are crucial to ensure the production of high-quality components.

Despite the potential for process optimisation, the use of new parameter combinations introduces the risk of defects. To mitigate this risk, a binary classifier designed for supervised anomaly detection can be integrated into the optimisation loop. In this context, a Random Forest Classifier (RFC) is chosen due to its superior performance in solving classification problems compared to standard decision trees [63]. It also exhibits competitive performance compared to more advanced methods such as neural networks [64], especially for the small datasets typical of manufacturing processes. On the other hand, it can result in overfitting problems, occurring when a model excels on the training data but encounters challenges when confronted with new unseen data. To address this issue within the RFC algorithm, several strategies can be employed. One approach involves limiting the depth of trees through tree pruning, which ensures a shallower tree structure. Additionally, increasing the minimum samples per leaf helps restraining the creation of nodes with very few instances, thereby diminishing the risk of capturing noise. Another effective technique is to curtail the number of features considered for each split in a tree. These precautionary measures could prevent individual trees from becoming overly specialised and aids in promoting a more generalised and robust model. In the presented case study, after a trial-and-error procedure that accounted for the overfitting problem, the best hyperparameters found were 10 trees in the forest, with a minimum of 5 samples per leaf, and up to 2 features in each tree.

2.5. Data-driven optimisation procedure

2.5.1. Genetic algorithm

The GA is a metaheuristic optimisation algorithm inspired by Darwin's evolutionary theory and genetics, which mimics the evolution process to identify optimal solutions without using gradients and differentiation of cost functions. GA is largely employed to solve diverse combinatorial optimisation problems also in the field of welding technology, trying to get welds with higher penetration depth and minimum number of deposited materials [65,66]. However, limited research has explored their application in the global minimisation of functions dependent on continuous variables and their application in GMA-AM process. In this study, an approach based on continuous GA [67] is proposed. This continuous GA, when coupled with a model based on GPR, proves effectiveness in determining optimal values, thanks to the exploration of capabilities of continuous GA and the interpolation capability of the GPR model.

GA employs three baseline processes, namely the "selection," the "crossover," and the "mutation" to iteratively improve randomly generated candidate solutions. Crossover involves swapping values of two distinct parameters, while mutation introduces small perturbations in the parameters. The generated solutions then undergo an evaluation, in which their fitness values are calculated. Higher values signify superior solutions, thus guiding through the selection phase. The exploration of better solutions is achieved through crossover and mutation processes.

To implement a continuous GA approach, several modifications to the traditional GA were introduced. First, all parameters are normalised based on observed minimum and maximum values. Therefore, the initial population (N) of the first generation follows a standard distribution with zero mean and a variance of 1, where 0 corresponds to the minimum value of control actions and 1 to the maximum value, namely wire feed speed, welding speed, welding voltage and frequency parameter called UltimArc in Lincoln system.

Crossover is performed by sampling two random indices within the parameter range, and their values are exchanged. Mutation introduces white noise with a fixed standard deviation (mutation gain), generating a noise vector that follows the distribution but results in different mutations for each parameter. To gradually reduce the impact of crossover and mutation as the algorithm progresses towards the optimum solution, a linear decrement is applied until the rates reach the minimum fixed values. This linear decrement facilitates the transition from exploration to exploitation throughout the optimisation process. The best candidate is then scaled using Eq. 7, where p are the parameters, o are the actions generated by the continuous GA and UB and LB the upper bound and lower bound vectors, respectively.

$$p = o \cdot (UB - LB) + LB \quad (7)$$

This approach allows for better initialisation of the action space with similar scales for all variables, avoiding illogical combinations, such as 0.5 m/min wire feed speed, 19 V, and 8 mm/s welding speed, which would likely result in no welding or even burnback, as the wire would melt faster than it is fed into the process. The scaling process is therefore mandatory for the computation of the fitness function, which employs the GPR and RFC models to evaluate the specific power consumption, the bead geometry, and the anomaly detection output. A summary of the hyperparameters of the continuous GA is reported in Table 1.

2.5.2. Fitness function design

The objective of the optimisation problem is encapsulated in the fitness function, in which the aim is to minimise power consumption. Notably, parameters such as WFS, frequency (UltimArc) and welding voltage are strictly linked to arc voltage and current, thereby influencing power consumption and the associated cost. Furthermore, the process parameters are also related to the final surface roughness [68], due to their correlation with layer geometry. By increasing the welding speed, the surface roughness can be reduced, thus resulting in a smoother layer deposition. Accordingly, the total energy consumption can be reduced, since the energy required per millimetre of the printed component (see Eq. 8) depends on the deposition speed. Moreover, this metric is

Table 1
Hyperparameters employed in the proposed continuous Genetic Algorithm and values.

Parameter	Population size	Generations	Ini. crossover rate	Ini. mutation rate	Ini. mutation gain
Value	50	100	0.6	0.6	0.05

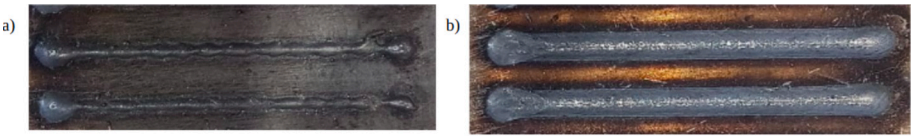

Fig. 6. a) Layers deposited with wrong process parameters (b) Layers deposited with correct process parameters.

particularly relevant as it enables generalisability across different components once their deposition length is known. It is also widely adopted in life cycle assessment studies to quantify the energy contribution per manufactured part.

$$SEC\left[\frac{J}{mm}\right] = 1000 \cdot \frac{PAI}{WS}\left[\frac{\frac{J}{mm \cdot s}}{s}\right] \tag{8}$$

On the other hand, it would also increase the chances of humping defects on the surface. Nevertheless, the reduction of surface roughness could also be achieved by reducing the wire feed speed, which also reduces the overall power consumption, enabling a linear reduction in the welding current [69]. In this context, it is evident that the optimisation task could be complex in finding the best trade-off between increasing welding speed and reducing wire feed speed for smoother layers, minimised energy consumption and at the same time avoiding defective layer. Addressing this multifaceted problem is challenging, and employing ML with GA optimisation, leverages exploration capabilities to discover novel solutions.

Considering all the aforementioned factors, a multi-objective fitness function is proposed and expressed in Eq. 9. In particular, if the process parameters are related to a deposition without any anomaly, the fitness function needs to be designed to increase when lower power consumption. At the same time, the agent should encourage to use of higher welding speed to reduce the deposition time, the SEC and smooth the surface roughness, while employing a lower wire feed speed at the same time. However, the lowest fitness function value has to be obtained if an anomaly is present. All the inputs of the fitness function are scaled with respect to the maximum values obtained during the experimental investigation.

$$f(p, WFS, WS) = \begin{cases} -\beta \cdot \frac{p}{p_{max}} - \frac{\beta}{2} \cdot \left(\frac{WFS}{WFS_{max}} - \frac{WS}{WS_{max}} \right) - \frac{\beta}{4} \cdot \frac{w}{w_{max}} \cdot \frac{h}{h_{max}}, & \lambda = 0 \\ -4\beta & \lambda = 1 \end{cases} \tag{9}$$

In the proposed fitness function, λ is the output of anomaly detection output (0 for normal deposition and 1 for an anomalous deposition). p is the PAI measured in kW, the *WS* is the welding speed, *WFS* is the wire feed speed and w and h are the layer width and height. The β value is used to modify the amplitude of the fitness function and is equal to 2 for the specific case.

3. Results and discussion

After conducting the experiments, the correlation between process parameters and output variables was first studied. Section 3.1 presents the results of the correlation analysis. Section 3.2 describes the training and validation of the regression and classification models by focusing on the performance across different datasets through cross-validation and analysis. In Section 3.3, the results of the proposed optimisation procedure are presented. To evaluate the impact of the proposed AI-driven regression–classification framework on process optimisation, three optimisation strategies are compared:

- Traditional optimisation without ML integration: a baseline approach relying exclusively on experimental observations from the best available dataset.
- Model-based ML optimisation without classification: an optimisation method employing ML regression models to predict process parameters, without accounting for layer quality.
- Proposed multi-model regression–classification ML optimisation: the complete methodological proposal introduced in this work, which integrates regression and classification models to simultaneously predict process parameters and assess layer quality during optimisation.

This integrated regression–classification strategy represents a novel methodological contribution of the present work. Unlike conventional AM optimisation methods, which typically rely either on regression-based prediction or purely data-driven parameter tuning, the proposed framework establishes a hybrid optimisation paradigm where predictive accuracy and quality assurance are jointly embedded in the optimisation loop. By comparing the three methods, the study quantifies the added value of AI, particularly the role of the classification stage, in enhancing optimisation robustness and consistency. The results of this comparison are presented in Section 3.4, demonstrating how the proposed approach outperforms traditional and regression-only strategies.

3.1. Preliminary statistical analysis of the collected data

Before proceeding with regression analysis, the statistics of the dataset and the correlation index computed using Spearman Correlation Index (SCI) are summarised in Table 2. As suggested by the correlation analysis, the *PAI* indicator was strongly dependent on *WFS* and *V*, since they mainly influence the heat input produced by the arc. Although there was not a high correlation with the UltimArc parameter, which influences the frequency content of the waveform, it can be observed in Fig. 7 that a non-linear trend between this input parameter and power consumption exists. Moreover, the data shows that a high correlation between *WS* and layer geometry exists, as extensively documented in literature (see e.g. [70,71]). However, there seems to be no influence on *PAI*, since it does not appear as any term in the formulation of Eq. 1 proposed by [55]. Nonetheless, this parameter strictly influences the deposition time, which is straightforwardly related to the global power consumption and hence the whole impact of the process. Concerning the layer geometry, the relationship between process parameters and layer geometry is well known from the literature [72–75]. As reported in Table 1, the increment of *WS* led to reduced layer geometries in terms of both layer width and layer height, while increasing either the *WFS* or the voltage led to reduced layer geometries. Furthermore, these parameters are the primary factors influencing power consumption and material deposition rate, as demonstrated by Shah et al. [76]. In particular, by increasing the *WFS* and the welding voltage, an increment of *PAI* is obtained. The statistical analysis confirms both the relationships and the signs used in the fitness function proposed in the previous chapter, as well as the feasibility of using the identified parameters to model the process.

3.2. Results of regression and classification models

In order to guarantee a stable deposition process, regression and binary classification analyses were conducted and used together to create the environment for the optimiser using two distinct ML approaches (GPR and RFC). The regression analysis was evaluated using K-fold cross-validation to assess the model's generalisation capability, with Mean Absolute Error (MAE) as the performance metric. This approach enables evaluation of the modelling technique's effectiveness and its sensitivity to the dataset, with low MAE variance across folds indicating good model performance. A low MAE allows for trustworthy exploration of the effect of the process parameters combination by GA optimisation algorithm, guaranteeing the same performance on the real system. Concerning the classification model, the employed metrics were precision (p), recall (re), accuracy (a) and *F2*-score, listed in Eqs. 10–13. Precision, recall, and *F2*-scores are essential metrics for evaluating classification models. Precision assesses the accuracy of detected anomalies, addressing false alarms, while recall measures the ability to identify all actual anomalies, addressing missed detections. The *F2*-score emphasises recall, making it particularly valuable in additive manufacturing, where avoiding missed anomalies outweighs the cost of false alarms due to the potential impact on process quality.

Table 2
Statistics of the collected dataset and correlation analysis between process parameters input and process output in terms of layer geometry and power consumption.

Features	Standard deviation	Mean value	Min value	25 %	50 %	75 %	Max value
UltimArc [−]	5.9	0.346	−10.0	−4.0	0.	4.0	10.0
Welding Speed [mm/min]	89.29	608.67	550.0	552.0	552.0	742.0	750.0
Wire Feed Speed [m/min]	1.82	4.7	2.0	3.0	4.5	6.5	6.5
Welding Voltage [V]	4.0	19.91	14.7	16.0	20.0	23.0	28.0
PAI [kW]	1.91	3.8	1.1	2.1	3.87	5.1	7.88
Layer width [mm]	1.8	6.05	3.2	4.05	6.5	7.52	9.9
Layer height [mm]	0.47	1.98	1.1	1.6	2.0	2.3	3.5
		SCI PAI		SCI Layer width		SCI Layer height	
UltimArc [−]		−0.1		−0.007		−0.024	
Welding Speed [mm/min]		0.12		−0.17		−0.22	
Wire Feed Speed [m/min]		0.89		0.92		0.85	
Welding Voltage [V]		0.88		0.80		0.57	

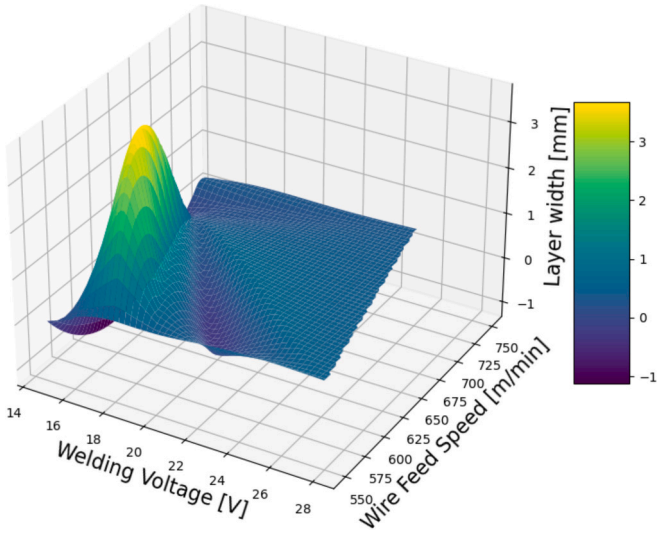

Fig. 7. Surface response plot of UltimArc and WFS process parameters with PAI index.

$$p = \frac{TP}{TP + FP} \tag{10}$$

$$re = \frac{TP}{TP + FN} \tag{11}$$

$$F2 = \frac{(1+\beta^2)\cdot p \cdot re}{\beta^2 \cdot p + re} = \frac{5p \cdot re}{4p + re} \tag{12}$$

$$a = \frac{TP + TN}{TP + FN + TN + FP} \tag{13}$$

3.2.1. Regression model performance

Before training the GPR model, the target vectors were normalised within the range of 0–1 to ensure the same scale for all predictors, to improve performance. During the training, the K-fold cross-validation method has been employed to evaluate the model's generalizability with $K = 10$. The results are discussed in terms of Mean Absolute Error (MAE) between prediction and target, and the average values of the metrics with the confidence interval obtained from the GPR are reported in Table 3.

The results showed a good capability of the model in estimating outcomes related to *PAI* and welding geometry. In particular, the model demonstrated good precision in predicting power, with an average MAE of 0.33 ± 0.14 *kW* across the K-folds. These values represent around 6 % deviation from the maximum value of 5.4 kW and 9 % from the mean value of 3.5 kW. Similar performance was observed for layer width, with an average MAE of 0.36 ± 0.17 *mm*, constituting 3.6 % of the maximum value and 6 % of the mean value. High accuracy was observed for layer height, with an average MAE of 0.18 ± 0.05*mm*, corresponding to 5 % and 9 % of the maximum and mean values, respectively. However, these deviations remain acceptable within the context of the study objectives.

Regarding the confidence interval, the analysis revealed that the average confidence interval for predictions across all folds is approximately 10 %, with a standard deviation of 0.3 %. This highlights the model's reliability and the consistency of its uncertainty estimates.

Table 3
Results obtained using K-fold cross-validation method for Regression model consisting of Gaussian Process Regression.

GPR metrics	PAI [kW]	Layer width [mm]	Layer height [mm]
Mean Absolute Error	0.33 ± 0.14	0.36 ± 0.17	0.18 ± 0.05
Confidence interval from GPR model	0.10 ± 0.03		

3.2.2. Classification model performance

The same K-fold procedure has been employed for evaluating the classification performance. However, given the class imbalance problem, the class weighting approach is employed based on the work of King et al. [77]. This approach assigns different weights to classes during the model training with the aim to penalise errors in minority classes, encouraging the model to treat all classes more equally, even if some are underrepresented. The results are reported in Table 4 in terms of mean and standard deviation values of the obtained precision, recall and *F2*-score. Moreover, given the binary classification nature of the anomaly detection problem, the ROC-AUC (Receiver Operating Characteristic - Area Under the Curve) metric is computed. The scikit learn Python library is used for all metric evaluations using the available functions.

The K-fold cross-validation results for the RFC model highlight its strong performance overall. A mean precision of 90.0 % and a recall of 77 % indicate the tendency of the model to miss some anomalies. However, the *F2*-score of 78.8 % reflects a reasonable result, particularly considering the imbalanced nature of the dataset. The mean accuracy of 94.3 % confirms the model's robust overall prediction capability, while the mean ROC-AUC of 94.3 % underscores its good discriminative capability. Although variability across the k-fold splits introduces some fluctuations in performance, the results remain consistently good.

Table 4
Results obtained using k fold method in developing the Random Forest Classifier.

RFC metrics	Precision	Recall	F2-score	Accuracy	ROC-AUC
Mean value	90.0 %	77.1 %	78.8 %	94.3 %	94.3 %
Standard deviation value	10 %	12 %	11 %	7 %	7 %

However, the observed standard deviation values suggest potential for further enhancement, particularly by increasing the representation of defective layers in the dataset. The current imbalance, with relatively few defective samples compared to defect-free ones, limits the model's ability to generalise fully to anomalous conditions.

3.3. Results of the metaheuristic optimisation

As highlighted in the introduction, nowadays, most optimisation techniques involving the selection of process parameters are based on experimental evidence. For this reason, this work compares the results of the proposed AI-based methodology with a manual optimisation. Furthermore, the results are compared with a state-of-the-art optimisation procedure in which no classifier is employed to estimate the output quality of the set of process parameters employed by the agent. To be more specific in relation to the effective fitness function employed in this study, given the normalisation applied to the outputs of the GPR model, the fitness function presented in Eq. 8 is modified into the form shown in Eq. 14, as scaling by the maximum value is no longer necessary. In particular, the normalised output of the GPR model ($p_{GPR}, w_{GPR}, h_{GPR}$) and the normalised output of the GA optimised (WFS_{GA}, WS_{GA}) are used together with the output of the RFC (λ_{RFC}).

$$f = \begin{cases} -\beta \cdot p_{GPR} - \dfrac{\beta}{2} \cdot (WFS_{GA} - WS_{GA}) - \dfrac{\beta}{4} \cdot w_{GPR} \cdot h_{GPR}, & \lambda_{RFC} = 0 \\ -4\beta & \lambda_{RFC} = 1 \end{cases} \tag{14}$$

3.3.1. Traditional optimisation without ML integration

Following a traditional method for this task, the experimental evidence led to the selection of parameters of layers 53 or 54 from the Table A.1 as possible optimal solution. In Table 5 are listed the process parameters and the related fitness function values obtained using the function designed in this work.

The fitness function shows that the best function is obtained by employing a lower welding voltage, which did not compromise the quality of the layer, combined with the highest welding speed and a wire feed speed of 3 m/min. In fact, by employing either a lower welding voltage, e.g. 14.7 V, or a lower wire feed speed, e.g. 2 m/min, the experimental evidence suggested that defects will always be present.

3.3.2. State-of-the-art: model-based ML optimisation without classification

While the results of traditional optimisation methods are satisfactory, the use of AI-powered optimisation techniques can further improve the fitness function and refine the outcomes. This can be achieved by implementing smart search strategies for process parameters and utilising a robust model that predicts outputs based on the parameters used. To demonstrate the limitation of the state of the art methods, an example is presented in which the optimisation is employed without the inclusion of the anomaly classifier. In this case, process parameters were used to predict the response variables, and optimisation was performed using a GA, which represents a more advanced technique compared to conventional response surface methodology.

The optimal condition was reached after a few iterations, yielding a final fitness function value of +0.12 with the following parameters: −10 UltimArc setting, welding speed of 750 mm/min, wire feed speed of 2 m/min, and welding voltage of 14.7 V. Although the optimisation procedure was faster and simpler, the absence of a classifier meant that the search space was not properly constrained in a non-linear manner, as in the surface response approach. Consequently, the algorithm could converge towards parameter combinations that optimise energy consumption but are unsuitable for production, as shown in Fig. 8. In this specific case, the algorithm tended to minimise power consumption by minimising the wire feed speed and excessively increasing the welding speed, which adversely affected the melting pool dynamics and led to a humping defect [78]. Therefore, the actual fitness value, considering the presence of the defect detected by the classifier is equal to −8, as shown in Table 6.

3.3.3. Proposal: multi-model regression–classification ML optimisation

As discussed above, although it is well documented that ML methods can be employed to solve optimisation tasks, without the formulation of a proper environment, the quality of the components printed under specific parameter combinations is not guaranteed. Therefore, in this work, a different approach to optimise the process parameters of GMA-AM is proposed, by relying on the use of an AM-oriented fitness function together with additional classification models to synthesise the environment. This combination allowed the avoidance of the production of defective parts, aiming to reduce the number of experiments needed for the optimisation.

Fig. 9 illustrates the result of the proposed optimisation algorithm at each generation. Thanks to exploration allowed by mutation and crossover operations, the action space is explored until an optimal condition is reached with a final fitness function value of −0.12 employing as parameters a − 4 UltimArc, a welding speed of 732 mm/min, a wire feed speed of 2.8 m/min and a welding voltage of 14.7 V. To avoid humping defect, the welding speed is reduced and to employ a lower welding voltage without the presence of anomalies, a higher wire feed speed has been employed, slight lower to the minimum acceptable value obtained from experimental evidence.

The proposed framework not only identifies energy-efficient process parameter combinations but also ensures defect-free deposition, as demonstrated by the experimental validation. Importantly, this integrated optimisation strategy revealed non-intuitive parameter configurations—such as low wire-feed speed combined with high travel speed—that would typically be excluded based on empirical practice. Nevertheless, the model-based optimisation confirmed that these configurations yield stable process behaviour and enhanced energy efficiency, underscoring the capability of the proposed approach to uncover optimal regions of the parameter space that conventional experimental methods may overlook.

3.4. Comparison of the results of the different optimisation techniques

Table 7 reports the results obtained for the three compared optimisation methods, in which the optimised process parameters are used to deposit layers on the plate according to the experimental investigation. To better highlight the obtained results, the PAI index was converted to SEC index expressed in J/mm, dividing the effective PAI for the welding speed.

In order to test the predictive performance of the models, the layer geometry was also measured for the new deposited layers and the real *PAI* was then evaluated. The deposition was repeated twice to evaluate the robustness of the results. Finally, the layer quality was assessed by visual inspection and audio signal from an expert. The experimental evidence consisted of selecting the best set from the experimental investigation, which resulted in a SEC of 167.36 J/mm.

By employing the standard technique without using the classifier for

Table 5
Optimum process parameters to employ based on experimental evidence of the proposed experimental investigation.

Layer	UltimArc	Wire feed speed [m/min]	Welding speed [mm/min]	Welding voltage [V]	PAI [kW]	Layer width [mm]	Layer height [mm]	Fit value
53	10	3	750	16	2.1	4.8	1.7	−0.32
54	−10	3	750	16	2.0	3.2	1.7	−0.28

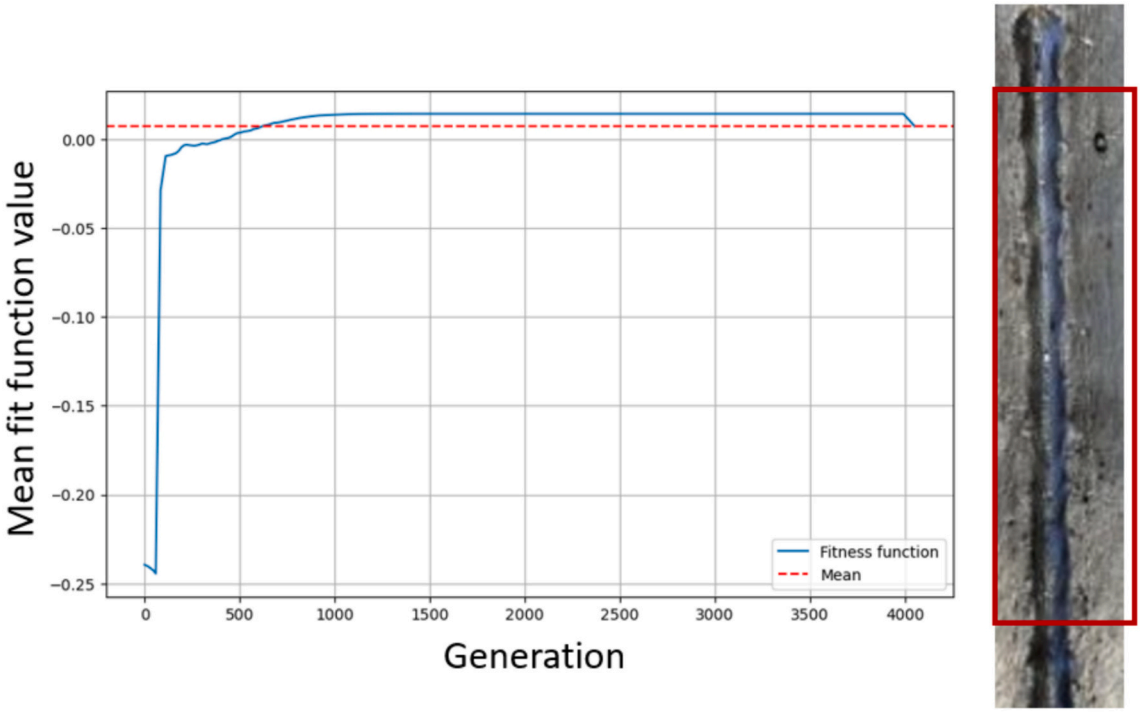

Fig. 8. Behaviour of fitness function along generation without using the Random Forest Classifier during the optimisation. The maximum value is reached in fewer iterations than the proposed case, and the process parameters lead to an anomaly.

Table 6
Effect of the presence of the classifier on fitness function evaluation. If the classifier is not used it is always assumed that $\lambda = 0$.

Layer	UltimArc	Wire feed speed [m/min]	Welding speed [mm/min]	Welding voltage [V]	PAI [kW]	Layer width [mm]	Layer height [mm]	Fit value
Without classifier	−10	2	750	14.7	1.55	3	1.1	+0.12
With classifier								−8

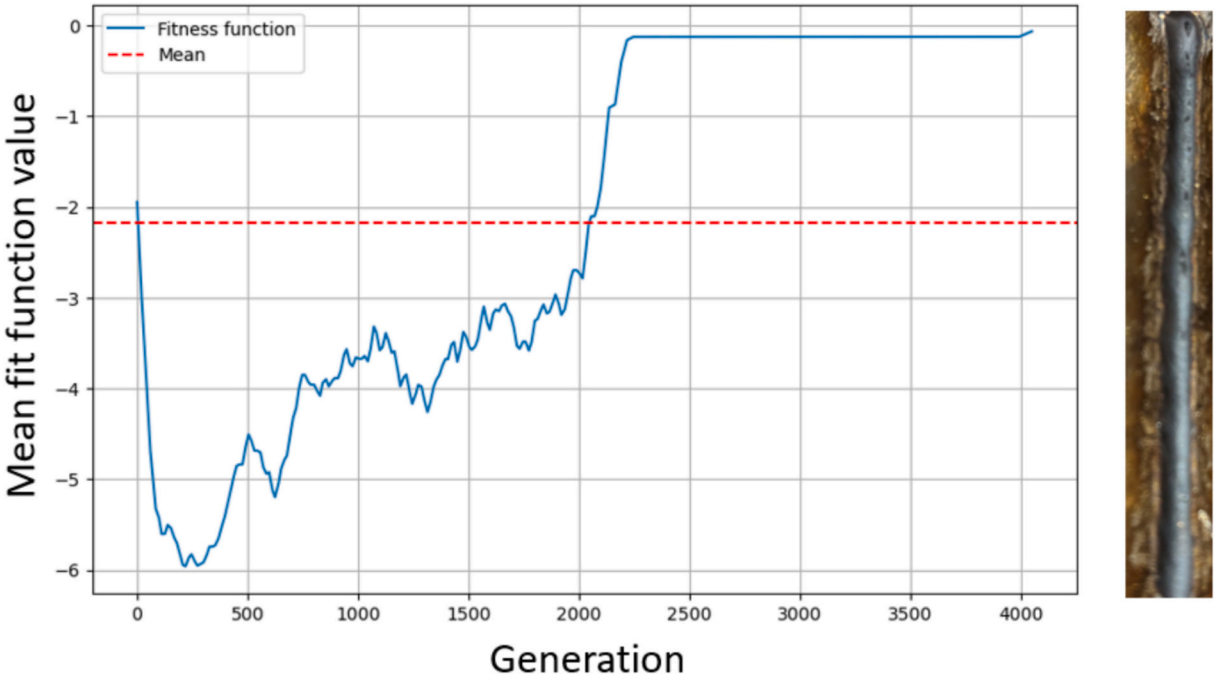

Fig. 9. Behaviour of fitness function along generation. Once the best process parameters are reached, the fitness function is fixed to the maximum value.

Table 7
Comparison of the results obtained with the three compared Optimisation Methods (OM).

Strategy	Estimated PAI [kW]	Real PAI [kW]	Estimated layer width [mm]	Real layer width [mm]	Estimated layer height [mm]	Real layer height [mm]	SEC [J/mm]	Real fit value
Traditional optimisation without ML	–	2.1	–	3.2	–	1.7	167.3	−0.28
ML optimisation – no classifier	1.25	1.55	3.3	3.0	1.3	1.1	124.6	−8
Multi-ML-model –with classifier	1.6	1.7	3.8	3.5	1.4	1.4	143.2	+0.024

the optimisation, a *PAI* of 1.25 kW and a predicted layer geometry of 3.2 and 1.3 mm was obtained by the proposed model, with results close to the real measured values of 1.55 kW, 3.0 mm and 1.1 mm. The resulting SEC index is 124.6 J/mm. In this case the real fit value is equal −8, since a humping defect occur during the deposition. Although a reduction of 25 % of power consumption was reached, a surface defect occurred during the deposition. Aiming to solve this issue, a new strategy based on a different environment was proposed to take into account the presence of defects.

In this case, using the proposed strategy, the predicted *PAI* by GPR was 1.6 kW with respect to the real 1.7 kW. The predicted layer width and height were, respectively 3.8 mm and 1.4 mm, with respect to the real values of 3.5 mm and 1.4 mm. The overall deposition led into a SEC of 124.6 J/mm, which reduced the power consumption by 14 % with respect to experimental evidence. This represents a good compromise with respect to the defined goal objective of this work.

The results presented in Table 7 also illustrate the differences between the model-predicted outputs and the actual values measured after deposition, highlighting the strong predictive performance of the models discussed in Section 3.2.

Finally, it is important to note that without the classification model for constructing the environment, the GA provides an optimal solution after 500 iterations, which ultimately proves to be the least effective among the various proposals. Including the classification models makes the optimisation process more complex, and the proposed algorithm required 28 min to reach a solution after more than 2000 iterations. Nevertheless, the results obtained demonstrated improved performance from an energy reduction perspective.

4. Testing on a complex component, limitations and future works

4.1. Printing component with AI-optimised process parameters

The AI-optimised process parameters enable the deposition of a single-layer with reduced energy consumption and improved surface smoothness. Although this optimisation procedure has been conducted on a simple single-layer deposition, the results of the optimisation are also valid for multi-layer fabrication of components with complex geometries. To demonstrate these capabilities, the proposed model, namely the developed GPR-RFC, was employed to print the component shown in Fig. 10a. Given the GA-optimised process parameters, the predicted layer height is 1.3 mm. Therefore, for a component with a total height of 20 mm, 14 layers were deposited, slicing the part based on this predicted layer height. The component was filled using a raster pattern strategy, as illustrated in Fig. 10b, with alternating orientations between odd and even layers, while the contour was printed only once per layer. The step-over distance (SOD), defined as the distance between two adjacent passes, was calculated using the estimated layer width predicted by the model under the optimised process parameters, specifically $\hat{w} = 3.8\,mm$. Applying the formula described by Ding et al. [74] based on the TOM model, the bead set step-over distance was determined as $SOD = 0.738, \hat{w} = 2.8\,mm$. During the printing process, the welding current and the welding voltage have been collected, allowing for measurement of the total energy consumed during the printing process.

To print the proposed component, the interpass temperature for the component was maintained at 25 °C, effectively minimising the influence of thermal gradients on layer geometry and ensuring consistent deposition stability across successive layers, minimising thermal-related geometry shifts introduced by changes of arc length due to changes in layer height [19,79]. Therefore, during the deposition, an interpass temperature of 25 °C is used, and a thermal camera is employed to measure the interpass temperature to start the following deposition, as shown in Fig. 11. The proposed thermal management strategy enabled the extension of the single-layer deposition model to multi-bead, multi-layer fabrication, as the distortion effects caused by heat accumulation were significantly reduced. To validate this approach, the layer height of the component was measured after each deposition, showing minimal variation, within the declared layer height error range, between the predicted and the actual component geometry.

The total energy consumed during the production of the component was measured as 2.32 MJ over a total arc-on time of 1339 s. On average, the contour printing phase requires approximately 24 s, while the infill stage takes around 76 s per layer, depending on whether the deposited layer index is odd or even, yielding an average build time of approximately 100 s per layer. The average energy was measured as 42 kJ for the contour and 132 kJ for the infill. Consequently, the measured average SEC per layer was 142.5 J/mm, which deviates by only 0.7 J/

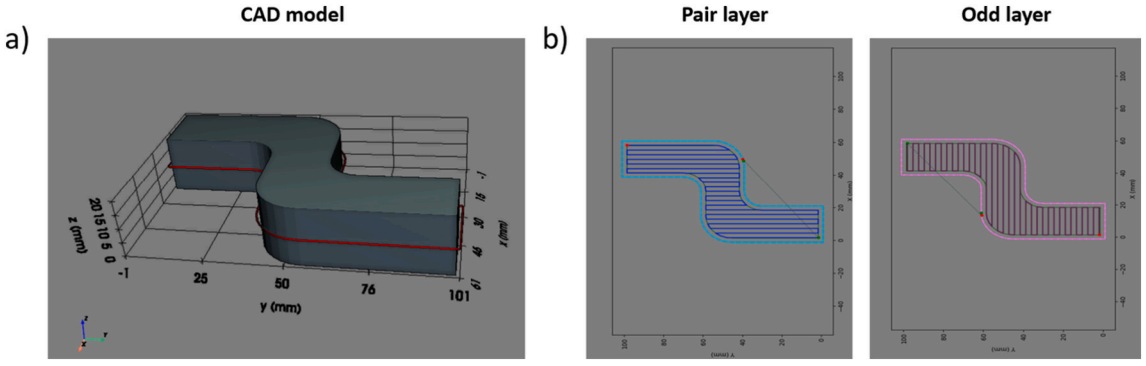

Fig. 10. The component printed in this study (a) the CAD model, (b) the deposition strategy.

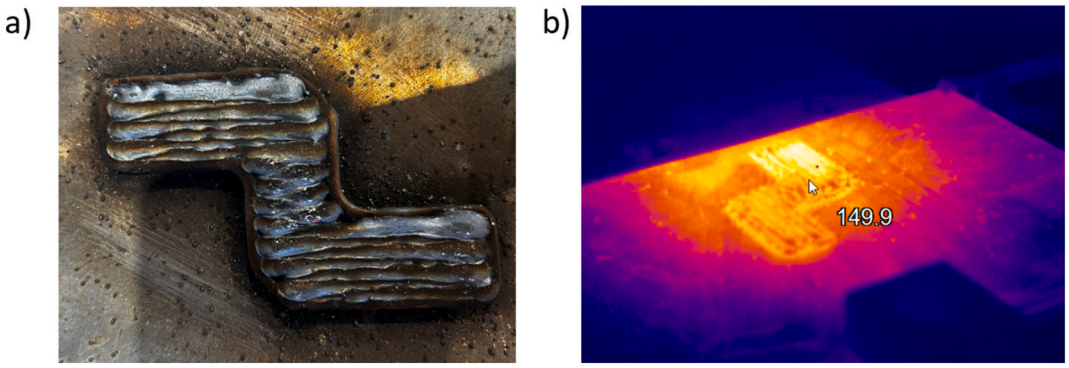

Fig. 11. (a) An example of an as-printed layer (b) measurement of interpass temperature via thermal camera.

mm from the value estimated by the developed machine learning model. This close agreement confirms also for the power consumption model the reliability of the model and supports its use in optimisation procedures.

The key metrics of the deposition process in terms of time and energy consumption have been reported in Table 7. Based on the total travel length of 16.34 m and the estimated SEC for the traditionally experimental-based optimised parameters, the total energy required without AI-based optimisation is estimated at 2.73 MJ. Therefore, with the implementation of AI-driven optimisation, this is reduced to 2.32 MJ, resulting in an energy saving of 405 kJ, equivalent to a 15 % reduction.

Moreover, the experimental validation confirms that the optimised parameters ensure stable arc behaviour and consistent layer formation across multiple layers, effectively avoiding defective conditions. These results validate the proposed approach as a reliable and sustainable optimisation strategy for GMA-AM, improving energy efficiency while preserving component quality.

4.2. Final discussion and future works

While ML techniques are widely used to estimate layer geometry, this study shows that GPR can also accurately predict average power consumption and, by extension, the SEC. Despite a small discrepancy of 0.7 J/mm, the model proved reliable for optimisation and suitable for integration into a slicer environment. Validation on a real component confirmed the accuracy of training-phase metrics computed on single-layer deposition also for multi-layer one. The findings suggest that AI-based optimisation, even when trained on single-layer data, remains valid for full-scale components, enabling significant time and cost savings. Indeed, the use of AI enabled a 15 % reduction in the energy consumption of the printed component, highlighting the tangible benefits of such techniques in supporting part design. However, it is worth noting that the proposed regression–classification framework is model-agnostic, and its novelty lies in the integration strategy rather than in the specific choice of algorithms; hence, while GPR and RFC were employed in this study for their interpretability and robustness with limited data, the same framework could seamlessly incorporate deep learning models in future developments, for example if generative AI is used for dataset augmentation [80,81].

Table 7
Summary of the printed component and deviations from the ML-predicted outcome.

Metric	ML-estimated	Measured	Deviation	Remarks
Total Energy Consumption (MJ)	–	2.32 MJ	–	Directly measured over total arc-on time
Arc-On Time (s)	–	1339 s	–	Duration for component production
Contour Time per Layer (s)	–	~24 s	–	Average measured duration
Infill Time per Layer (s)	–	~76 s	–	Depends on odd/even layer index
Total Time per Layer (s)	–	~100 s	–	Sum of contour and infill times
Average Power (Contour) (kJ)	–	42 kJ	–	Based on actual measurements
Average Power (Infill) (kJ)	–	171 kJ	–	Based on actual measurements
Specific Energy Consumption (J/mm)	143.2 J/mm	142.5 J/mm	0.7 J/mm	Excellent agreement validates ML model reliability for optimisation purposes

Future work will focus on multi-layer, multi-bead structures, enabling the evaluation of additional parameters, such as step-over distance, on surface quality. This will also allow for mechanical testing, providing further inputs for the development of more comprehensive, data-driven optimisation models. Moreover, a main assumption of this study is the controlled thermal management during experiments, with the interpass temperature maintained at 25 °C to minimise thermal effects on layer geometry. While this condition validated the optimisation framework scaling from single-layer to multi-layer components, different thermal interactions can affect bead shape and residual stresses. Therefore, future work should integrate thermal effects into the predictive and optimisation models, enabling reliable optimisation under variable interpass temperatures and removing the constant-temperature assumption. Despite these limitations, the primary objective of the study, which is enhancing sustainability by reducing energy consumption, was successfully achieved.

Another promising direction would be to integrate the proposed optimisation algorithm into a slicing software. Beyond the welding parameters, different deposition strategies (e.g., path planning and infill orientation) also influence the overall energy consumption. For example, by exploring the effects of infill angle or overlapping distance on the overall SEC could offer valuable insights. Such investigations could enhance the optimisation process by jointly considering process parameters and deposition strategies. Since the proposed models are already capable of estimating energy consumption once the SEC is known, this integration appears feasible and could lead to more comprehensive and intelligent optimisation workflows. This would mark a shift from purely predictive modelling towards a more holistic and practical application within digital manufacturing pipelines.

5. Conclusion

This work proposed a novel AI-based optimisation framework for the Pulsed Gas Metal Arc Additive Manufacturing process, integrating regression and classification models within a metaheuristic Genetic

Algorithm to enhance process sustainability. By combining a Gaussian Process Regression model with a Random Forest Classifier, the framework predicts power consumption, layer geometry, and quality while automatically constraining unstable parameter regions, addressing a key limitation of existing optimisation approaches. The introduction of a sustainability-oriented fitness function enables the discovery of more energy efficient process parameter combinations beyond experimentally validated configurations. The optimised parameters achieved smoother layers and a 14 % reduction in energy consumption, with experimental validation on a multi-bead and multi-layer printed component confirming a 15 % decrease in total energy use. These findings demonstrate that the proposed framework can effectively guide parameter selection towards energy-efficient and high-quality fabrication. Future work will extend this approach to multi-layer depositions, incorporating different thermal management strategies during deposition and including additional outputs such as mechanical and surface properties derived from varying process parameters. This will enable a more comprehensive optimisation and establish robust process boundaries. Furthermore, the integration of this AI-driven optimisation methodology into slicing software will facilitate its practical adoption in industrial Additive Manufacturing environments.

CRediT authorship contribution statement

Giulio Mattera: Writing – review & editing, Writing – original draft, Visualization, Software, Methodology, Investigation, Formal analysis, Data curation, Conceptualization. **Zengxi Pan:** Writing – review & editing, Writing – original draft, Resources, Methodology, Investigation, Funding acquisition, Data curation. **Luigi Nele:** Writing – review & editing, Writing – original draft, Supervision, Project administration, Investigation, Funding acquisition, Conceptualization. **Vittoria Laghi:** Writing – review & editing, Writing – original draft, Visualization, Methodology, Investigation, Formal analysis, Conceptualization.

Declaration of competing interest

The corresponding author Giulio Mattera declares to accept responsibility for all statements listed below:

- All authors have given their contribution in the drafting of this original paper;
- All authors concur with the submission;
- I have taken the consent from all co-Authors before publishing the present article in this journal
- The manuscript has not been submitted to another journal and will not be published elsewhere within one year.
- All authors have no financial/commercial conflict of interest of any kind to disclose.

Appendix A

Table A.1
Table of experiments.

N layer	UltimArc	Welding speed [mm/min]	Wire feed speed [m/min]	Welding voltage [V]	PAI [kW]	Layer width [mm]	Layer height [mm]	Anomaly
1	−8	552	6.5	23	5.44	7.85	2.2	0
2	−6	552	6.5	23	5.49	7.73	2.5	0
3	−4	552	6.5	23	5.41	7.55	2.4	0
4	−2	552	6.5	23	5.51	7.7	2.5	0
5	2	552	6.5	23	5.63	8.5	3.5	0
6	4	552	6.5	23	5.32	7.93	3	0
7	6	552	6.5	23	5.39	7.75	2.3	0
8	8	552	6.5	23	5.36	8	2.3	0
9	0	552	6.5	18	4.26	6.5	2.6	1
10	0	552	6.5	20	4.69	7.4	2	1
11	0	552	6.5	28	7.70	8.2	2.4	0
12	4	552	6.5	28	5.53	8	2	0
13	4	552	6.5	20	4.56	8	2.1	0
14	4	552	6.5	18	4.55	9.9	2.1	1
15	−4	552	6.5	18	3.96	6.6	2.7	1
16	−4	552	6.5	28	4.23	6.9	2.6	0
17	−4	552	6.5	20	7.52	8	2.2	0
18	8	552	6.5	20	4.46	6.7	2.6	0
19	8	552	6.5	28	7.36	8.4	2.1	0
20	8	552	6.5	18	4.08	6.4	2.5	1
21	−8	552	6.5	18	4.28	8.4	2.4	1
22	−8	552	6.5	28	7.78	7.9	2.3	0
23	−8	552	6.5	20	4.67	7.5	2.2	0
24	2	552	6.5	20	4.73	7.5	2.4	0
25	2	552	6.5	28	7.78	8.8	2.4	0
26	2	552	6.5	18	4.42	6.7	3	1
27	−2	552	6.5	18	4.39	6.8	2.4	1
28	−2	552	6.5	28	7.88	8.1	2	0
29	−2	552	6.5	20	4.89	7.8	2.7	0
30	0	552	4.5	23	3.77	6.8	1.6	0
31	4	552	4.5	23	3.64	6.6	1.8	0
32	−4	552	4.5	20	3.68	6.4	1.9	0
33	−4	552	4.5	23	4.32	6.3	2	0
34	4	552	4.5	20	3.43	6.2	2.1	0
35	0	552	4.5	20	3.54	6.5	2.1	0
36	0	552	4.5	18	3.13	5.5	2.1	0

(*continued on next page*)

Table A.1 (*continued*)

N layer	UltimArc	Welding speed [mm/min]	Wire feed speed [m/min]	Welding voltage [V]	PAI [kW]	Layer width [mm]	Layer height [mm]	Anomaly
37	−4	552	4.5	18	3.11	5.8	2.2	0
38	4	552	4.5	18	3.09	5.7	2.2	0
39	0	552	4.5	23	4.13	6.1	1.9	0
40	4	552	4.5	23	4.17	6.3	2	0
41	4	552	4.5	20	3.47	6.6	2	0
42	0	552	4.5	20	3.47	6.6	2.2	0
43	0	552	4.5	18	3.11	5.6	1.9	0
44	4	552	4.5	18	3.14	5.6	2.2	0
45	4	750	6.5	25.2	6.23	7.2	2	0
46	4	750	4.5	21	3.78	5.8	1.8	0
47	−4	750	6.5	25.2	6.43	7.4	1.9	0
48	−4	750	4.5	21	3.87	6.3	1.9	0
49	8	750	4.5	21	3.73	6.7	1.8	0
50	8	750	6.5	25.2	6.23	7.1	1.8	0
51	−8	750	6.5	25.2	6.55	7.4	2	0
52	−8	750	4.5	21	3.91	5.5	2	0
53	0	750	3	16	2.11	4.2	1.8	0
54	10	750	3	16	2.09	4.8	1.7	0
55	−10	750	3	16	2.11	3.2	1.7	0
56	0	750	2	14.7	1.36	3.2	1.6	1
57	10	750	2	14.7	1.33	3.4	1.2	1
58	−10	750	2	14.7	1.31	3.8	1.2	1
59	−10	550	2	14.7	1.39	3.2	1.1	1
60	0	550	2	14.7	1.45	3.5	1.4	1
61	10	550	2	14.7	1.40	3.3	1.4	1
62	10	550	3	16	2.14	4.4	1.6	0
63	−10	550	3	16	2.17	4.6	1.3	0
64	0	550	2	16	1.12	3.8	1.5	1
65	0	750	2	16	1.27	3.4	1.3	1
66	−10	550	2	16	1.10	3.7	1.4	1
67	10	550	2	16	1.29	3.9	1.5	1
68	4	750	2	16	1.42	3.4	1.3	1
69	−4	750	2	16	1.43	3.4	1.3	1
70	−10	750	2	16	1.15	3.3	1.3	1
71	10	750	2	16	1.36	3.5	1.4	1
72	4	550	2	16	1.47	3.8	1.5	1

References

[1] Dilberoglu UM, Gharehpapagh B, Yaman U, Dolen M. The role of additive manufacturing in the era of Industry 4.0. Procedia Manuf 2017;11:545–54. https://doi.org/10.1016/j.promfg.2017.07.148.

[2] Norrish J, Polden J, Richardson I. A review of wire arc additive manufacturing: development, principles, process physics, implementation and current status. J Phys D Appl Phys 2021;54(47):473001. https://doi.org/10.1088/1361-6463/ac1e4a.

[3] Wang Q, et al. A review on energy consumption and efficiency of selective laser melting considering support: advances and prospects. Int J Precis Eng Manuf-Green Technol 2024;11(1):259–76. Jan. https://doi.org/10.1007/s40684-023-00542-3.

[4] Pan Z, Ding D, Wu B, Cuiuri D, Li H, Norrish J. Arc Welding Processes for Additive Manufacturing: A Review. 2018. p. 3–24. https://doi.org/10.1007/978-981-10-5355-9_1.

[5] Mu H, Polden J, Li Y, He F, Xia C, Pan Z. Layer-by-layer model-based adaptive control for wire arc additive manufacturing of thin-wall structures. J Intell Manuf 2022;33(4):1165–80. Apr. https://doi.org/10.1007/s10845-022-01920-5.

[6] Xiong J, Zhang Y, Pi Y. Control of deposition height in WAAM using visual inspection of previous and current layers. J Intell Manuf 2021;32(8):2209–17.

[7] Xia C, et al. Model predictive control of layer width in wire arc additive manufacturing. J Manuf Process 2020;58:179–86.

[8] Mattera G, Caggiano A, Nele L. Optimal data-driven control of manufacturing processes using reinforcement learning: an application to wire arc additive manufacturing. J Intell Manuf. 2025;36:1291–310.

[9] Mattera G, Polden J, Caggiano A, Commins P, Nele L, Pan Z. Anomaly detection of wire arc additively manufactured parts via surface tension transfer through unsupervised machine learning techniques. In: 17th CIRP Conference on Intelligent Computation in Manufacturing Engineering. Naples: Procedia CIRP; 2023.

[10] Li Y, et al. A defect detection system for wire arc additive manufacturing using incremental learning. J Ind Inf Integr 2022;27:100291. https://doi.org/10.1016/j.jii.2021.100291.

[11] Xia C, Pan Z, Li Y, Chen J, Li H. Vision-based melt pool monitoring for wire-arc additive manufacturing using deep learning method. Int J Adv Manuf Technol 2022;120(1–2):551–62. May, https://doi.org/10.1007/s00170-022-08811-2.

[12] Gao H, et al. Towards quality controllable strategies in wire-arc directed energy deposition. Aug. 01. Institute of Physics; 2025. https://doi.org/10.1088/2631-7990/adb9a9.

[13] Cai Y, Xiong J, Chen H, Zhang G. A review of in-situ monitoring and process control system in metal-based laser additive manufacturing. J Manuf Syst 2023;70:309–26. Oct. https://doi.org/10.1016/J.JMSY.2023.07.018.

[14] Liu H, Chen H, Xiong J. Abnormal melt pool behavior in overhead wire arc-based directed energy deposition. J Manuf Process 2025;150:1164–77. Sep. https://doi.org/10.1016/J.JMAPRO.2025.07.020.

[15] Cai Y, Li C, Chen H, Xiong J. Towards automatic anomaly detection and diagnosis in positional arc-directed energy deposition based on deep learning. J Manuf Syst 2025;79:1–13. Apr. https://doi.org/10.1016/J.JMSY.2024.12.015.

[16] Mattera G, Vozza M, Polden J, Nele L, Pan Z. Frequency informed convolutional autoencoder for in situ anomaly detection in wire arc additive manufacturing. J Intell Manuf 2024:1–16.

[17] Franke J, Heinrich F, Reisch RT. Vision based process monitoring in wire arc additive manufacturing (WAAM). J Intell Manuf 2025;36(3):1711–21. https://doi.org/10.1007/s10845-023-02287-x.

[18] Li R, et al. Application of unsupervised learning methods based on video data for real-time anomaly detection in wire arc additive manufacturing. J Manuf Process 2025;143:37–55. Jun, https://doi.org/10.1016/j.jmapro.2025.03.113.

[19] Chen D, Chen H, Zhang G, Xiong J. Towards automatic control of process stability for thick-wall parts in arc-directed energy deposition based on arc voltage sensing. J Manuf Process 2025;141:250–62. May, https://doi.org/10.1016/J.JMAPRO.2025.03.008.

[20] Kumar A, Sadhya S, Khan AU, Madhukar YK. Improvement in process efficiency of WAAM-TIG by in-situ voltage–current–temperature monitoring and feedback control system. Int J Precis Eng Manuf Jul. 2025;26(7):1673–81. https://doi.org/10.1007/s12541-024-01208-z.

[21] Bernauer C, et al. Segmentation-based closed-loop layer height control for enhancing stability and dimensional accuracy in wire-based laser metal deposition. Robot Comput Integr Manuf 2024;86:102683. Apr, https://doi.org/10.1016/j.rcim.2023.102683.

[22] He F, et al. Research and application of artificial intelligence techniques for wire arc additive manufacturing: a state-of-the-art review. Robot Comput Integr Manuf 2023;82:102525. https://doi.org/10.1016/j.rcim.2023.102525.

[23] Mattera G, Paolela D, Nele L. Monitoring and control the wire arc additive manufacturing process using artificial intelligence techniques: a review. J Intell Manuf 2024;35:467–97.

[24] Priarone PC, Campatelli G, Catalano AR, Baffa F. Life-cycle energy and carbon saving potential of Wire Arc Additive Manufacturing for the repair of mold inserts.

CIRP J Manuf Sci Technol 2021;35:943–58. https://doi.org/10.1016/j.cirpj.2021.10.007.
[25] Hegab H, Khanna N, Monib N, Salem A. Design for sustainable additive manufacturing: a review. Sustain Mater Technol 2023;35:e00576. Apr, https://doi.org/10.1016/j.susmat.2023.e00576.
[26] Dupont JN, Marder AR. Thermal efficiency of arc welding processes. Weld J 1995; 74 [Online]. Available: https://api.semanticscholar.org/CorpusID:17702193.
[27] Dias M, Pragana JPM, Ferreira B, Ribeiro I, Silva CMA. Economic and environmental potential of wire-arc additive manufacturing. Sustainability 2022; 14(9):5197. Apr, https://doi.org/10.3390/su14095197.
[28] Priarone PC, Pagone E, Martina F, Catalano AR, Settineri L. Multi-criteria environmental and economic impact assessment of wire arc additive manufacturing. CIRP Ann 2020;69(1):37–40.
[29] Kokare S, et al. Wire arc additive manufacturing of a high-strength low-alloy steel part: environmental impacts, costs, and mechanical properties. Int J Adv Manuf Technol 2024. https://doi.org/10.1007/s00170-024-14144-z. Jul.
[30] Liu Z, Zhao Y, Wang Q, Xing H, Sun J. Modeling and assessment of carbon emissions in additive-subtractive integrated hybrid manufacturing based on energy and material analysis. Int J Precis Eng Manuf-Green Technol 2024. https://doi.org/10.1007/s40684-023-00588-3. Jan.
[31] Campatelli G, Montevecchi F, Venturini G, Ingarao G, Priarone PC. Integrated WAAM-subtractive versus pure subtractive manufacturing approaches: an energy efficiency comparison. Int J Precis Eng Manuf-Green Technol 2020;7(1):1–11. Jan, https://doi.org/10.1007/s40684-019-00071-y.
[32] Wurst J, Steinhoff T, Mozgova I, Hassel T, Lachmayer R. Aspects of a sustainability focused comparison of the wire arc additive manufacturing (WAAM) and the laser powder bed fusion (LPBF) Process. 2023. p. 88–97. https://doi.org/10.1007/978-981-19-9205-6_9.
[33] Laghi V, Savino E, Gasparini G. Reduction of the environmental impact of complex-shaped steel joints through topology optimization and large-scale metal 3D printing. Res Eng Des 2025:105610. https://doi.org/10.1016/j.rineng.2025.105610.
[34] Cozzolino E, Astarita A. Energy saving in milling of electron beam–melted Ti6Al4V parts: influence of process parameters. Int J Adv Manuf Technol 2023;127(1–2): 179–94. https://doi.org/10.1007/s00170-023-11502-1.
[35] Cozzolino E, Franchitti S, Borrelli R, Pirozzi C, Astarita A. Energy consumption assessment in manufacturing Ti6Al4V electron beam melted parts post-processed by machining. Int J Adv Manuf Technol 2023;125(3–4):1289–303. Mar, https://doi.org/10.1007/s00170-022-10794-z.
[36] Zavdoveev A, et al. Optimization of the pulsed arc welding parameters for wire arc additive manufacturing in austenitic steel applications. Int J Adv Manuf Technol 2022;119(7–8):5175–93. Apr, https://doi.org/10.1007/s00170-022-08704-4.
[37] Wani ZK, Abdullah AB, Jaafar NA, Hussain Z. Multi-stages, multi-responses optimisation of wire arc additive manufacturing parameters using Taguchi method. Mater Today Proc 2022;66:2660–4. https://doi.org/10.1016/j.matpr.2022.06.490.
[38] Justus Panicker CT, Rohit Surya K, Senthilkumar V. Novel process parameters based approach for reducing residual stresses in WAAM. Mater Today Proc 2022; 59:1119–26. https://doi.org/10.1016/j.matpr.2022.03.025.
[39] Meng X, Weber B, Nitawaki M, Gardner L. Optimisation and testing of wire arc additively manufactured steel stub columns. Thin-Walled Struct 2023;189:110857. https://doi.org/10.1016/j.tws.2023.110857.
[40] Prasanna Nagasai B, Malarvizhi S, Balasubramanian V. A study on wire arc additive manufacturing of 308L austenitic stainless steel cylindrical components: optimisation, microstructure and mechanical properties. Proc Inst Mech Eng B J Eng Manuf 2023;237(9):1391–404. https://doi.org/10.1177/09544054221129471.
[41] Geng H, Li J, Xiong J, Lin X. Optimisation of interpass temperature and heat input for wire and arc additive manufacturing 5A06 aluminium alloy. Sci Technol Weld Join 2017;22(6):472–83. Aug, https://doi.org/10.1080/13621718.2016.1259031.
[42] Gihr M, Rashid A, Melkote SN. Bead geometry prediction and optimization for corner structures in directed energy deposition using machine learning. Addit Manuf 2024;84:104080. Mar, https://doi.org/10.1016/J.ADDMA.2024.104080.
[43] Liu H, Chen H, Zhang G, Pan Z, Xiong J. Complex-geometry metal parts in arc-directed energy deposition: Fabrication methods, defect formation mechanisms, quality improvement strategies. J Manuf Process 2025;155:379–400. Dec, https://doi.org/10.1016/J.JMAPRO.2025.10.044.
[44] Mattera G, Caggiano A, Nele L. Reinforcement learning as data-driven optimization technique for GMAW process. Weld World 2023. https://doi.org/10.1007/s40194-023-01641-0.
[45] Tomaz I do V, Colaço FHG, Sarfraz S, Pimenov DYu, Gupta MK, Pintaude G. Investigations on quality characteristics in gas tungsten arc welding process using artificial neural network integrated with genetic algorithm. Int J Adv Manuf Technol 2021;113(11–12):3569–83. Apr, https://doi.org/10.1007/s00170-021-06846-5.
[46] Katherasan D, Elias JV, Sathiya P, Haq AN. Simulation and parameter optimization of flux cored arc welding using artificial neural network and particle swarm optimization algorithm. J Intell Manuf 2014;25(1):67–76. Feb, https://doi.org/10.1007/s10845-012-0675-0.
[47] Xiong J, Zhang G, Hu J, Wu L. Bead geometry prediction for robotic GMAW-based rapid manufacturing through a neural network and a second-order regression analysis. J Intell Manuf 2014;25(1):157–63.
[48] Ding D, He F, Yuan L, Pan Z, Wang L, Ros M. The first step towards intelligent wire arc additive manufacturing: an automatic bead modelling system using machine learning through industrial information integration. J Ind Inf Integr 2021;23: 100218. Sep, https://doi.org/10.1016/j.jii.2021.100218.
[49] Kumar A, Maji K. Selection of process parameters for near-net shape deposition in wire arc additive manufacturing by genetic algorithm. J Mater Eng Perform 2020; 29(5):3334–52. May, https://doi.org/10.1007/s11665-020-04847-1.
[50] Le VT, et al. Prediction and optimization of processing parameters in wire and arc-based additively manufacturing of 316L stainless steel. J Braz Soc Mech Sci Eng 2022;44(9):394. Sep, https://doi.org/10.1007/s40430-022-03698-2.
[51] Le Van T, et al. Optimizing process stability and energy efficiency in wire arc additive manufacturing of nickel-based superalloys using machine learning. Int J Adv Manuf Technol 2025. https://doi.org/10.1007/s00170-025-15748-9. May.
[52] Yuan L, et al. Investigation of humping phenomenon for the multi-directional robotic wire and arc additive manufacturing. Robot Comput Integr Manuf 2020;63: 101916. Jun, https://doi.org/10.1016/j.rcim.2019.101916.
[53] Ramalho A, Santos TG, Bevans B, Smoqi Z, Rao P, Oliveira JP. Effect of contaminations on the acoustic emissions during wire and arc additive manufacturing of 316L stainless steel. Addit Manuf 2022;51:102585. Mar, https://doi.org/10.1016/j.addma.2021.102585.
[54] Mattera G, Polden J, Norrish J. Monitoring the gas metal arc additive manufacturing process using unsupervised machine learning. Weld World 2024: 1–15.
[55] Joseph A, Harwig D, Farson DF, Richardson R. Measurement and calculation of arc power and heat transfer efficiency in pulsed gas metal arc welding. Sci Technol Weld Join 2003;8(6):400–6. Dec, https://doi.org/10.1179/136217103225005642.
[56] Norrish J. Recent gas metal arc welding (GMAW) process developments: the implications related to international fabrication standards. Welding in the World 2017;61(4):755–67. Jun, https://doi.org/10.1007/s40194-017-0463-8.
[57] Reis RC, Kokare S, Oliveira JP, Matias JCO, Godina R. Life cycle assessment of metal products: a comparison between wire arc additive manufacturing and CNC milling. Adv. Ind. Manuf. Eng 2023;6:100117. May, https://doi.org/10.1016/j.aime.2023.100117.
[58] Spreafico C, Kokare S, Godina R. Prospective life cycle assessment of future Wire Arc Additive Manufacturing deposition process for large-scale steel parts. Environ Impact Assess Rev 2026;116:108111. Jan, https://doi.org/10.1016/J.EIAR.2025.108111.
[59] Ulkir O, Bayraklılar MS, Kuncan M. Raster angle prediction of additive manufacturing process using machine learning algorithm. Appl Sci 2024;14(5): 2046. Feb, https://doi.org/10.3390/app14052046.
[60] Tapia G, Khairallah S, Matthews M, King WE, Elwany A. Gaussian process-based surrogate modeling framework for process planning in laser powder-bed fusion additive manufacturing of 316L stainless steel. Int J Adv Manuf Technol 2018;94 (9–12):3591–603. Feb, https://doi.org/10.1007/s00170-017-1045-z.
[61] Byrd RH, Lu P, Nocedal J, Zhu C. A limited memory algorithm for bound constrained optimization. SIAM J Sci Comput 1995;16(5):1190–208. Sep, https://doi.org/10.1137/0916069.
[62] Xiong J, Zhang G, Hu J, Wu L. Bead geometry prediction for robotic GMAW-based rapid manufacturing through a neural network and a second-order regression analysis. J Intell Manuf 2014;25(1):157–63.
[63] Singh A, N. M, Lakshmiganthan R. Impact of different data types on classifier performance of random forest, naïve bayes, and K-nearest neighbors algorithms. Int J Adv Comput Sci Appl 2017;8(12). https://doi.org/10.14569/IJACSA.2017.081201.
[64] Han T, Jiang D, Zhao Q, Wang L, Yin K. Comparison of random forest, artificial neural networks and support vector machine for intelligent diagnosis of rotating machinery. Trans Inst Meas Control 2018;40(8):2681–93. May, https://doi.org/10.1177/0142331217708242.
[65] Correia DS, Gonçalves CV, da Cunha SS, Ferraresi VA. Comparison between genetic algorithms and response surface methodology in GMAW welding optimization. J Mater Process Technol 2005;160(1):70–6. Mar, https://doi.org/10.1016/j.jmatprotec.2004.04.243.
[66] Nagesh DS, Datta GL. Genetic algorithm for optimization of welding variables for height to width ratio and application of ANN for prediction of bead geometry for TIG welding process. Appl Soft Comput 2010;10(3):897–907. Jun, https://doi.org/10.1016/j.asoc.2009.10.007.
[67] Chelouah R, Siarry P. A continuous genetic algorithm designed for the global optimization of multimodal functions. J Heuristics 2000;6:191–213 [Online]. Available: https://api.semanticscholar.org/CorpusID:17042441.
[68] Xia C, Pan Z, Polden J, Li H, Xu Y, Chen S. Modelling and prediction of surface roughness in wire arc additive manufacturing using machine learning. J Intell Manuf 2022;33(5):1467–82. Jun. https://doi.org/10.1007/s10845-020-01725-4.
[69] Zhao S, Qiu X, Burnett I, Rigby M, Lele A. A lumped-parameter model for sound generation in gas metal arc welding. Mech Syst Signal Process 2021;147:107085.
[70] Mu H, Polden J, Li Y, He F, Xia C, Pan Z. Layer-by-layer model-based adaptive control for wire arc additive manufacturing of thin-wall structures. J Intell Manuf 2022;33(4):1165–80.
[71] Mattera G, Paolela D, Nele L. Monitoring and control the wire arc additive manufacturing process using artificial intelligence techniques: a review. J Intell Manuf 2023.
[72] Bestard GA, Alfaro SCA. Automatic control of the Weld Bead Geometry. In: Welding-Modern Topics. IntechOpen London, UK; 2020. p. 1–23.
[73] Krishnaveni S, Kunchala BR, Gamini S, Ch Anilkumar T. Machine learning-based bead modeling of wire arc additive manufacturing (WAAM) using an industrial robot. Mater Today Proc 2023. https://doi.org/10.1016/j.matpr.2023.04.534. May.
[74] Ding D, Pan Z, Cuiuri D, Li H. A multi-bead overlapping model for robotic wire and arc additive manufacturing (WAAM). Robot Comput Integr Manuf 2015;31: 101–10.

[75] Kunchala BKR, Gamini S, Anilkumar TC. Inclusion of IoT technology in additive manufacturing: machine learning-based adaptive bead modeling and path planning for sustainable wire arc additive manufacturing and process optimization. Proc Inst Mech Eng C J Mech Eng Sci 2023;237(1):120–32. Jan, https://doi.org/10.1177/09544062221117660.

[76] Shah IH, Hadjipantelis N, Walter L, Myers RJ, Gardner L. Environmental life cycle assessment of wire arc additively manufactured steel structural components. J Clean Prod 2023;389:136071. Feb, https://doi.org/10.1016/j.jclepro.2023.136071.

[77] King G, Zeng L. Logistic regression in rare events data. Polit Anal 2001;9(2):137–63.

[78] Liu H, Wang S, Chen H, Xiong J. Drop and hump behaviors in robotic arc-directed energy deposition with vertical position. Addit Manuf 2024;82:104049. Feb, https://doi.org/10.1016/J.ADDMA.2024.104049.

[79] Shi M, Xiong J. Controlling torch height and deposition height in robotic wire and arc additive manufacturing on uneven substrate. Welding in the World 2024;68(4):765–79. Apr, https://doi.org/10.1007/s40194-023-01633-0.

[80] Li T, Cao Y, Ye Q, Zhang YM. Generative adversarial networks (GAN) model for dynamically adjusted weld pool image toward human-based model predictive control (MPC). J Manuf Process 2025;141:210–21. May, https://doi.org/10.1016/J.JMAPRO.2025.02.053.

[81] Mucllari E, Cao Y, Ye Q, Zhang Y. Modeling imaged welding process dynamic behaviors using Generative Adversarial Network (GAN) for a new foundation to monitor weld penetration using deep learning. J Manuf Process 2024;124:187–95. Aug, https://doi.org/10.1016/j.jmapro.2024.05.081.